ICARUS **129,** 539–554 (1997)
ARTICLE NO. IS975801

The Sticking Properties of Water Frost Produced under Various Ambient Conditions

Kimberley D. Supulver

Board of Studies in Astronomy and Astrophysics, University of California, Santa Cruz, California 95064
E-mail: supulver@ucolick.org

Frank G. Bridges, Salvador Tiscareno, and John Lievore

Department of Physics, University of California, Santa Cruz, California 95064

and

D. N. C. Lin

Board of Studies in Astronomy and Astrophysics, University of California, Santa Cruz, California 95064

Received March 15, 1996; revised June 13, 1997

To form planetary systems, small solid particles which condense out of the cooling gas of the primitive solar nebula must aggregate together to form larger bodies. Centimeter-sized particles can grow out of micrometer-sized grains; planets can form from the coagulation of kilometer-sized planetesimals. The formation of stable, long-lived kilometer-sized objects from centimeter-sized particles is, however, not so straightforward. Some sort of surface sticking force is needed to hold these aggregates together against rotational forces as well as collisions in a turbulent solar nebula. We have performed experiments to determine the surface sticking force of water frosts under a variety of ambient conditions. Our primary results are listed below.

1. The structure of the frost is critical in determining its sticking properties; thin, porous frosts are more likely to adhere than are thick, dense frosts.

2. Sticking forces range up to 250 dyn/mm^2.

3. Temperature fluctuations can increase the sticking force by significant amounts.

4. The frost bond acts like a spring: it stretches before breaking, with the displacement proportional to the applied force. Measured spring constants for many different water frosts cluster between 10^5 and 10^6 dyn cm^{-1} (over a total area of 78 mm^2).

Based on these findings, we suggest that frosts of volatiles such as water could provide the necessary surface sticking mechanism in some low-temperature regions of the solar nebula.

1. INTRODUCTION

Current theories hold that the planets formed from a disk of gas and dust orbiting the Sun (e.g., Cameron 1978, 1995). Such disks have been observed around other stars, and these disks are thought to be very commonplace around young stars with masses similar to that of the Sun (Beckwith and Sargent 1993). Recent detections of planetary companions around stars such as 51 Pegasi (Mayor and Queloz 1995), 70 Virginis (Marcy and Butler 1996), and 47 Ursae Majoris (Butler and Marcy 1996) suggest that planet formation may be a rather ubiquitous process. In these theories of planet formation, 10^4-km terrestrial planets and 10^4-km outer planet cores must form from the population of micrometer-sized grains that condense (Prinn and Fegley 1989) out of the cooling gaseous disk orbiting the central star. The aggregation of small objects into large clusters must therefore play an important role in the formation of planets and has been a topic of investigation for more than two decades (Safronov 1969, Kerridge and Vedder 1972, Hartmann 1978, Weidenschilling 1984, 1987, Weidenschilling and Cuzzi 1993). To reach millimeter sizes, researchers have used models in which van der Waals bonding between the grains provides weak binding forces (Weidenschilling 1980, Chokshi *et al.* 1993, Blum and Münch 1993). However, for an aggregate to grow larger and eventually form a planetesimal (a kilometer-sized object), some sort of surface sticking force above and beyond van der Waals bonding is required in the centimeter-to-meter size range to hold the growing body together against collisions with other particles (Weidenschilling and Cuzzi 1993). We propose that frosts which form on the surfaces of small particles in the outer nebula provide this sticking force.

From observations of molecular abundances in comets, which are considered to be essentially unaltered remnants

0019-1035/97 $25.00

from the era of Solar System formation, we have one measure of the abundances of various volatile molecules at the time of planetesimal formation and thus an indication of which molecules might play a role in surface sticking. Mumma *et al.* (1993) provide a detailed discussion of recent progress in detections of cometary volatiles. Note, however, that these volatiles come from the outer regions of comets, regions which have been altered somewhat by their long exposure to, for example, solar ultraviolet radiation and cosmic rays. The primary volatile constituent of comets is water (H_2O). Carbon monoxide (CO) has been detected in several comets at abundance levels (by number) ranging from several percent to 20% that of water. The abundance of methanol (CH_3OH), by comparison, is observed to be a few percent that of water (from 1–5%, depending on the comet). The carbon dioxide (CO_2) abundance in Comet Halley is 3% that of water. Other significantly abundant observed cometary molecules include formaldehyde (H_2CO) and methane (CH_4). Comets likely formed in a region near or beyond the Uranus–Neptune zone, at temperatures below ~60 K (Mumma *et al.* 1993). Most of the data presented here were taken at temperatures slightly higher than this; these data, therefore, while not directly applicable to comet formation, would be applicable to planetesimal formation in the Jupiter–Uranus region, where temperatures were somewhat higher.

Current theory suggests that the cores of the giant planets formed from ice-coated (H_2O, NH_3, CH_4, etc.) silicate and metal grains which accreted to form a 10^4-km diameter core (Encrenaz *et al.* 1987). During this process, the accreting bodies must have passed through the centimeter-to-meter size range, in which case surface sticking forces would have been important.

The satellites of the outer planets must also have formed from ice-coated particles. These satellites provide critical information on the abundances of H_2O, CO, and other molecules that were present in the nebula during their formation. Assuming elemental abundances from Anders and Grevesse (1989), the two most abundant condensible materials are silicates (which form ''rocks'') and water (which forms ''ice''). ''Rocks'' also include other refractories, such as iron; ''ice'' may contain, for example, CH_4 clathrate, CO_2 ice, CO clathrate, or other volatiles, depending on the temperature and pressure at which the ice formed (Lunine and Tittemore 1993). In addition, gases such as CO, CH_4, and N_2 could be dissolved in, for example, an amorphous H_2O ice matrix without forming a clathrate hydrate (Bar-Nun *et al.* 1988). Pressures in the outer solar nebula were probably too low for widespread clathrate formation (although clathrate formation might occur after planetesimal collisions), but significant clathration likely occurred during the formation of satellites in the higher-pressure nebulae surrounding the giant planets (Lunine and Stevenson 1985). The percentage of ice (by mass) in some of these satellites is estimated to be ≈25 to 70% (Lunine and Tittemore 1993), so ice must have played a significant role in their formation.

In this paper we report experimentally determined sticking forces for water frosts prepared under a variety of conditions in order to further understand the surface sticking process which must have occurred during planetesimal formation in the outer Solar System. (Frosts of other volatiles also exhibit sticking (Bridges *et al.* 1996).) In this experiment, the sticking forces we measure are elastic, not viscous; the short time scales of our experiment preclude the investigation of viscous effects. These sticking forces are large enough to hold centimeter-sized aggregates together against collisions at velocities up to ~10 cm sec^{-1} (depending on the particle masses and the surface properties of the frost).

2. EXPERIMENTAL DETAILS

2.1. Apparatus

The experiment is designed to measure the sticking force between two frost-coated plates for temperatures in the range 40–200 K. The apparatus is mounted inside an insert for a conventional dewar system which can use liquid nitrogen or liquid helium cryogenic fluids. The data presented here were collected at temperatures in the range 70–160 K using liquid nitrogen coolant.

The brass lower plate (the base plate in Fig. 1) is attached to stainless steel support rods and is fixed to the cryostat insert; it holds a heater and thermocouples for controlling and measuring the local temperature. The upper plate (the test plate), a small aluminum disk of area 0.785 cm^2, is suspended by a string (or fine wire) 66 cm long from a strain gauge load cell located at the top of the cryostat (Fig. 2). Other types of surface material (e.g., porous ceramic) can be fixed onto the metal surfaces. The entire apparatus is suspended on rubber vibration pads, and the cryostat is leveled such that the small upper plate is positioned over the center of the lower plate.

The load cell is used to measure forces on the upper plate; the output is calibrated over the range 0–150 g with an accuracy of 0.02 g. The observed force is the sum of the weight of the upper plate plus any sticking forces between the plates. When no frost is present and the plates are not in contact, the recorded force gives the weight of the upper plate. This assumes that the apparatus is very stiff compared to the support string. When the apparatus is under vacuum during a run, the forces exerted by the surrounding atmosphere on the top of the apparatus can be orders of magnitude greater than the sticking forces we measure. Consequently, there should be little displacement of this part of the apparatus when small forces, corresponding to ~30 g, are applied. We discuss the stiffness of the lower part of the apparatus in the next section.

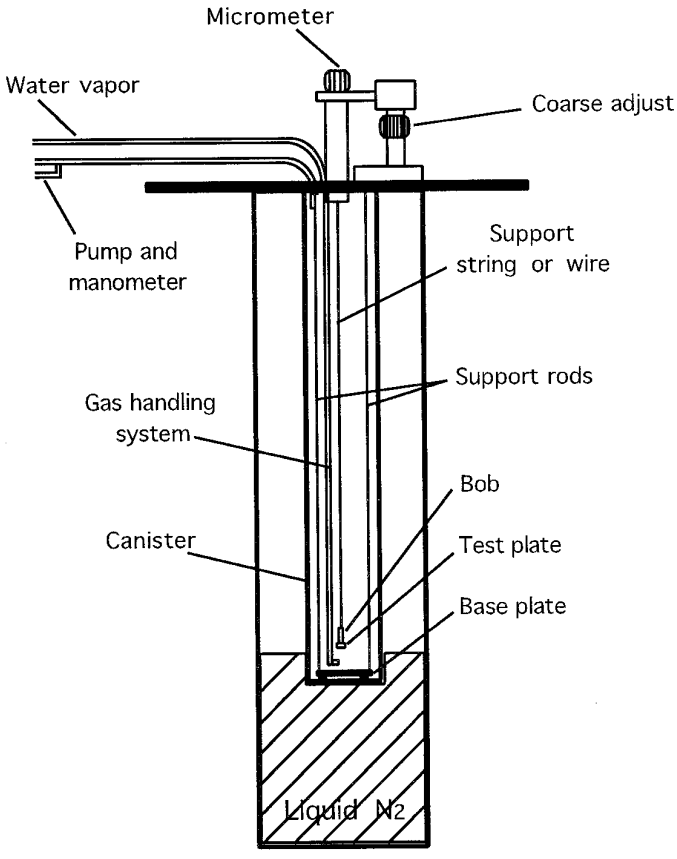

FIG. 1. A cutaway view of the apparatus used in these experiments.

The section of the apparatus containing the load cell can be raised and lowered a distance of 5 cm with a coarse control (resolution about 0.25 mm) and over a small range (0.5 cm) using a fine control. The resolution of the fine control motion is approximately 1.3 μm, which is achieved using a fine scale micrometer and a lever arrangement to reduce the motion of the load cell by a factor of 2 relative to the displacement of the micrometer (Fig. 2).

The suspended upper plate forms a simple pendulum and consequently can oscillate horizontally if displaced while raising or lowering the load cell. This motion must be eliminated before the two plates are brought into contact. In this apparatus, horizontal motion is damped magnetically; a magnet built into the lower plate induces currents in the upper aluminum plate which oppose mechanical motion. After the system is perturbed, the horizontal motion is completely damped in a few minutes. These induced forces are motion-dependent and are not relevant in static measurements.

For the sticking measurements, a source of water vapor is required near the plates. The water vapor is carried by nitrogen (or helium) gas, which bubbles through water at various flow rates; most data here were taken for frosts deposited at gas flow rates of 22 and 2.4 ml sec^{-1}. The water vapor/gas mixture passes through heated, insulated tubing to the bottom of the cryostat; the tubing (part stainless steel, part copper) is maintained at a temperature above 5°C to ensure that no frost forms on the tubing walls. Two nozzles at the bottom of the cryostat direct the flow of water vapor/gas in a horizontal direction about 1.5 cm above the lower plate.

2.2. *Procedures*

In operation, after the insert is mounted and the cryostat is cooled to the desired temperature for frost formation, the upper plate is raised to a position 3 cm above the lower plate using the coarse control. Frost is deposited on both plates for different deposition times, and in different ambient gas (nitrogen or helium) pressures, controlled by valves on the input line and the vacuum system (see Fig. 1). After frosting, the system returns to the ambient temperature

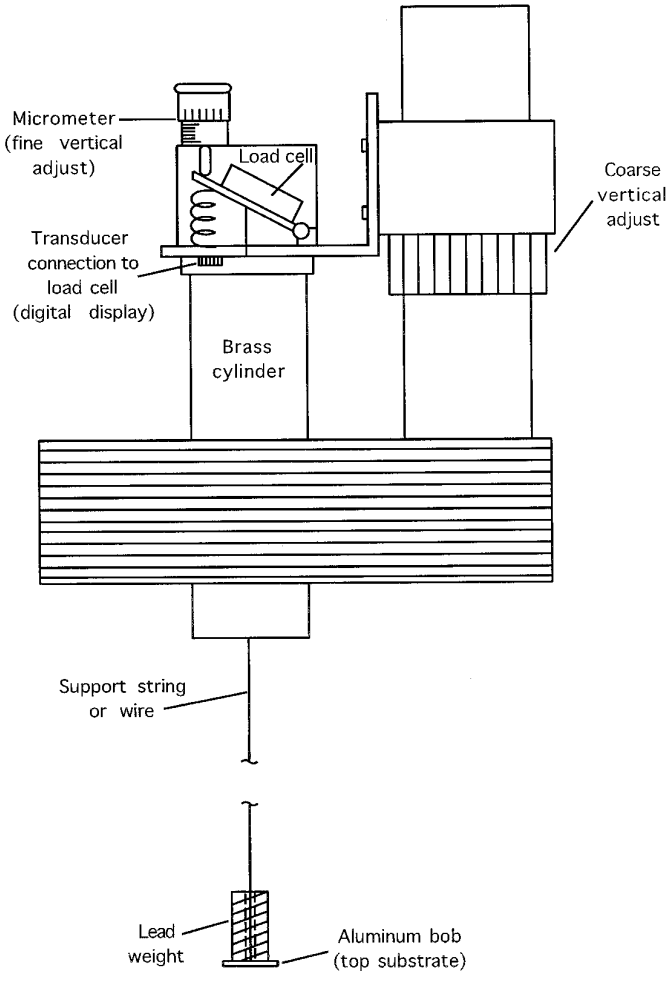

FIG. 2. A closer look at the micrometer and load cell system.

(the warm gas required for frosting raises the ambient temperature of the lower section by as much as 20 K for a long deposition), and the upper plate is then lowered to within 1 mm of the lower plate. The apparatus then sits undisturbed for several minutes to allow any horizontal motion to be damped. Next, the upper plate is lowered very slowly using first the coarse and then the fine controls until it is resting on the bottom plate. Once initial contact is achieved (i.e., once the reading on the load cell is ≈1 g below the weight of the plate), it takes several seconds to lower the plate until the load cell reading decreases to zero. This slow compression ensures that the frost is compacted only by the weight of the upper plate and not by deceleration forces which can be larger. Under these conditions, the upper plate is lowered at a rate of approximately 0.01 cm sec^{-1} over several seconds, which corresponds to an ''impact'' force of less than 1 dyn, a miniscule force compared to the weight of the upper plate (~1500 dyn for the 1.6 g mass). Additional weights can be set on the plate to increase the compressive force; for most of the results presented here, the net static compressive masses (plate plus weights) were 1.6, 16, and 22 g. A few experiments were also performed using a 110 g weight.

After the frost is compressed, the load cell is raised vertically, and the force is recorded as a function of the vertical position. First the fine support string (or wire) is stretched as the weight of the plate is taken up. If no sticking occurs, the force recorded by the load cell reaches the weight of the top plate and then remains constant. If sticking occurs, the force continues to increase as the load cell is raised. At some point the frost layer breaks and the measured force drops back to the weight of the upper plate. The maximum excess force, above the weight of the plate, is defined to be the sticking force. In this measurement, the frost layer also stretches and has an effective spring constant (Hatzes *et al.* 1991). To isolate the distance over which the frost stretches and determine the spring constant of the frost layer, the stretch of the support strand must first be measured under the same ambient conditions. The lower end of the support strand was held in place using a 100 g weight on the upper plate; forces in the appropriate range (e.g., from 10 to 30 g for experiments with the 16 g weight) were then applied and the stretch determined. For the polyester string, the force–displacement curve is linear, and we obtained the spring constant of the string from the slope, measured at low temperatures. The spring constant for various pieces of string varied by ≈12%. However, for the brass wire (diameter 0.5 mm), the relationship between force and distance was not linear over a wide range of applied force, due in part to small kinks in the wire and the support connection. Over small ranges of force the curve was close to linear and effective force constants were used. The top and middle panels of Fig. 3 show sample calibration curves for both the string and the wire.

To quantify the stiffness of the apparatus itself, we performed a calibration with the upper plate clamped to the brass plate. We measured the applied force both as the displacement increased and as it decreased (i.e., for both loading and unloading, respectively). The bottom panel of Fig. 3 shows that the applied force at a given displacement is nearly the same in both cases, within the estimated uncertainty in displacement indicated by the error bars. The solid line is a linear least-squares fit to the average of the applied forces for loading and unloading. This spring constant is very close to the K_s of the middle panel, in which the upper plate was not clamped to the brass plate; therefore, the apparatus is extremely stiff and does not contribute to the measured spring constant of the frost.

The frost and support strand act as two springs in series; the effective spring constant, K_{eff}, of the combination is

$$K_{eff} = \frac{K_f K_s}{K_f + K_s}, \tag{1}$$

where K_f and K_s are the spring constants of the frost and support strand, respectively. Therefore,

$$K_f = \frac{K_{eff} K_s}{K_s - K_{eff}}. \tag{2}$$

The maximum distance over which the frost stretches, δx_f, is given by

$$\delta x_f = \frac{F_s}{K_f}. \tag{3}$$

Using these equations and the calibration for K_s, we obtained, for each contact, the maximum sticking force, the spring constant of the frost, and the total stretch of the frost layer.

In some cases, the top plate was again lowered and the above experiment repeated several times, to see how the sticking force changed with the number of contacts. In others, more frost was deposited and the sticking measurement(s) repeated. These measurements were all carried out at a fixed temperature. In all cases, after one or more contacts, the surfaces no longer stuck together.

Another set of measurements was carried out in which the temperature was changed after the frost deposition. The question addressed is the following: Can a rise in temperature restore the sticking force? After no sticking was observed, the surfaces were brought together as described previously, and the temperature was raised from the initial temperature to approximately 130–180 K while the surfaces were pressed together under gravity. The top

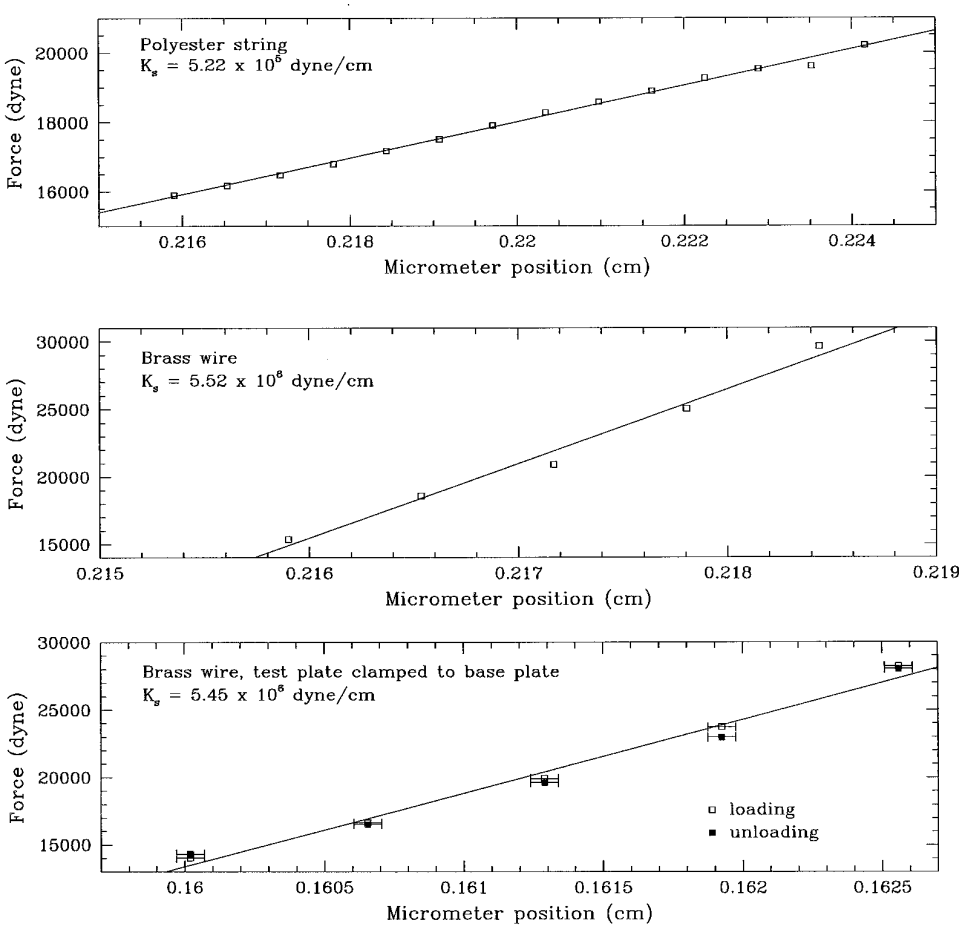

FIG. 3. Determination of the spring constant of two support strands: the polyester string and the brass wire (top and middle, respectively). The bottom panel shows the spring constant for the brass wire determined with the top plate clamped to the bottom plate. The errors in K_s for the top, middle, and bottom panels are $\pm 8.93 \times 10^3$, $\pm 4.00 \times 10^5$, and $\pm 3.96 \times 10^5$ dyn cm^{-1}, respectively. The error in position is ± 0.00005 cm in each case, as shown by the error bars in the bottom panel.

plate was then raised to determine whether or not sticking had occurred. (The total elapsed time after the first application of frost was typically 15–20 min.) In addition, some measurements were made in a similar fashion, but the surfaces were not separated after the first contact at the deposition temperature. In these cases, after deposition, the plates were brought together, the temperature raised, and the sticking force measured as the plates were separated at the elevated temperature.

3. RESULTS

3.1. Frost Thickness and Morphology

The water frost is deposited from a nitrogen or helium atmosphere with temperatures of order 100 K and pressures ranging from several Torr to approximately 400 Torr. For comparison, typical temperatures and total ambient gas pressures in the midplane of the solar nebula were $\approx$200 K and $\sim 10^{-4}$ Torr, respectively, in the region of Jupiter (5 AU) and $\approx$60 K and $\sim 10^{-5}$ Torr in the region of Neptune (30 AU) (Supulver 1997). The water vapor pressure in the nebula is $\approx 5 \times 10^{-4}$ times the total pressure, assuming solar abundances (Palme and Fegley 1990). However, in regions in which icy particles are actively sublimating, the water vapor pressure would be many orders of magnitude higher. The equilibrium vapor pressure over a solid at temperature T is given by

$$P_v = \exp[-\Delta G_{sub}/RT], \quad (4)$$

where ΔG_{sub} is the free energy of sublimation and R is the gas constant (Haynes *et al.* 1992). The free energy of sublimation $\Delta G_{sub} = \Delta H_{sub} - T\Delta S_{sub}$, where ΔH_{sub} is the enthalpy of sublimation and ΔS_{sub} is the entropy of sublimation. Haynes *et al.* (1992) derived $\Delta H_{sub} = 11.8$ kcal mol^{-1} and $\Delta S_{sub} = 31.0$ cal K^{-1} mol^{-1}. Using these values and $R = 1.99 \times 10^{-3}$ kcal K^{-1} mol^{-1},

$$P_v = \exp[-5940.0/T + 15.6] \text{ atm.} \quad (5)$$

At 200 K, the water vapor pressure is approximately 6×10^{-4} Torr, so P_v is comparable to the total ambient gas pressure in the nebula. At the sublimation temperature of water ice ($\approx$150 K), the vapor pressure drops to 3×10^{-8} Torr; water ice essentially does not sublimate below $\approx$150 K.

At the temperatures and pressures in our apparatus, the mean free path for water particles is orders of magnitude smaller than the spacing between the plates and the nozzle. Consequently, the vapor transport is via diffusion and convection. The multiple collisions cool the warm vapor/gas mixture that is injected into the low temperature environment. It is not clear, however, how the frost layer forms. The primary process could be direct condensation of water molecules onto the cold surfaces, but more likely, the deposition of small clusters (micro-snowflakes) plays a significant role. Dust particles within Saturn's rings or in the primordial solar nebula would provide nucleation sites for tiny snowflake clusters; the deposition of these tiny clusters on the surface over a long period of time would enhance the formation of a porous frost layer, which we have found to be advantageous for sticking.

To gain some knowledge of the deposition process, we have carried out frost depositions in a small, separate chamber in which the cold deposition surface is only a few centimeters below a warm viewing window. This allows visual observation using a low power microscope. However, the temperature gradients are much larger than in our sticking apparatus cryostat. In this small chamber we have noted that a fine fog forms in a region between the nozzles. Thus, although we have used clean nitrogen or helium as a carrier gas, tiny clusters tens of micrometers in size clearly do form. We have used this result to simulate the formation of dust-nucleated tiny snowflakes by depositing the frost in different ambient pressures to change the amount of nucleation. The morphology of the resulting frost layer depends on this deposition process. In particular, if 10–100 μm-sized snowflake clusters form and then are deposited onto the surfaces, the frost layers may be very porous and may have dendritic-like protrusions, which would enhance the sticking force in the "Velcro" model (see Section 3.4). In addition, images of the frost layer collected *in situ* in the sticking apparatus itself with an optical viewing system using a CCD camera clearly show a fluffy frost structure composed of many individual "whiskers," some of which may be dendritic ("tree-like") in nature. The whiskers form a complicated, interwoven criss-crossed structure, which gives rise to the "Velcro" effect.

The structure of the frost layer also changes with the amount of water vapor deposited. Consequently, the frost thicknesses are not well determined. For a flow rate of 22 ml sec^{-1}, 1.5–2 mm of frost are deposited in 20 min at a pressure of 25 Torr. At this thickness, the frost appears dense and the surface is very smooth, with variations below the 100 μm level. In contrast, frost layers formed at the same flow rate but for a shorter time (i.e., 2–4 min) appeared less dense, and irregularities and voids were easily visible. The thickness (defined as the greatest thickness of the frost) was larger than expected for the thin frosts but difficult to measure. For the longer deposition times, the vapor appears to move through, and deposit within, the porous initial layer, resulting in an increase in the density of the frost. A similar effect has been reported by Lock (1990) for frost deposited at much higher temperatures. As a result, in this paper we will describe our frost layers in terms of the deposition time for a fixed flow rate. Various flow rates did not change the general features described above, with one exception: at low pressures and a slow flow rate (e.g., $P < 25$ Torr and a flow rate of 2.4 ml sec^{-1} at a temperature of 104 K), a transparent layer of ice (likely amorphous ice) formed first. For such cases no sticking was observed. Eventually, for long enough depositions, islands of frost begin to form on this icy surface. (Here we make a distinction between an icy layer which is transparent and a porous frosty layer which appears white.) This regime has not yet been investigated as it requires long depositions (several hours or more).

At the temperatures and pressures considered here, clathrates should form readily for nitrogen gas. Miller (1961) determined the temperature dependence of the dissociation pressure of N_2 clathrate using a statistical–mechanical calculation,

$$\log_{10} P_{\text{atm}} = -763/T + 4.996, \quad (6)$$

where T is in degrees Kelvin. At 100 K, the dissociation pressure $P \approx 2$ Torr; therefore, we expect N_2 clathrate to form at the higher pressures in our experiment. To check that the sticking is not strongly dependent on the nitrogen clathrate, we used helium as a carrier gas and measured the sticking forces at temperatures near 100 K. Helium clathrate is not expected to form at helium pressures (fugacities) below $\sim 10^4$ bar (Lunine and Stevenson 1985). These experiments gave essentially the same results as those using nitrogen as the carrier gas. We conclude that clathrate formation plays at most a secondary role unless it predetermines the morphology of the frost.

3.2. *A Typical Sticking Force Measurement*

The maximum sticking force, the effective spring constant, and the maximum stretch of the frost just prior to breaking have been measured for a wide range of conditions for water-frost coated surfaces. In each case the sticking measurement procedure is the same as that described

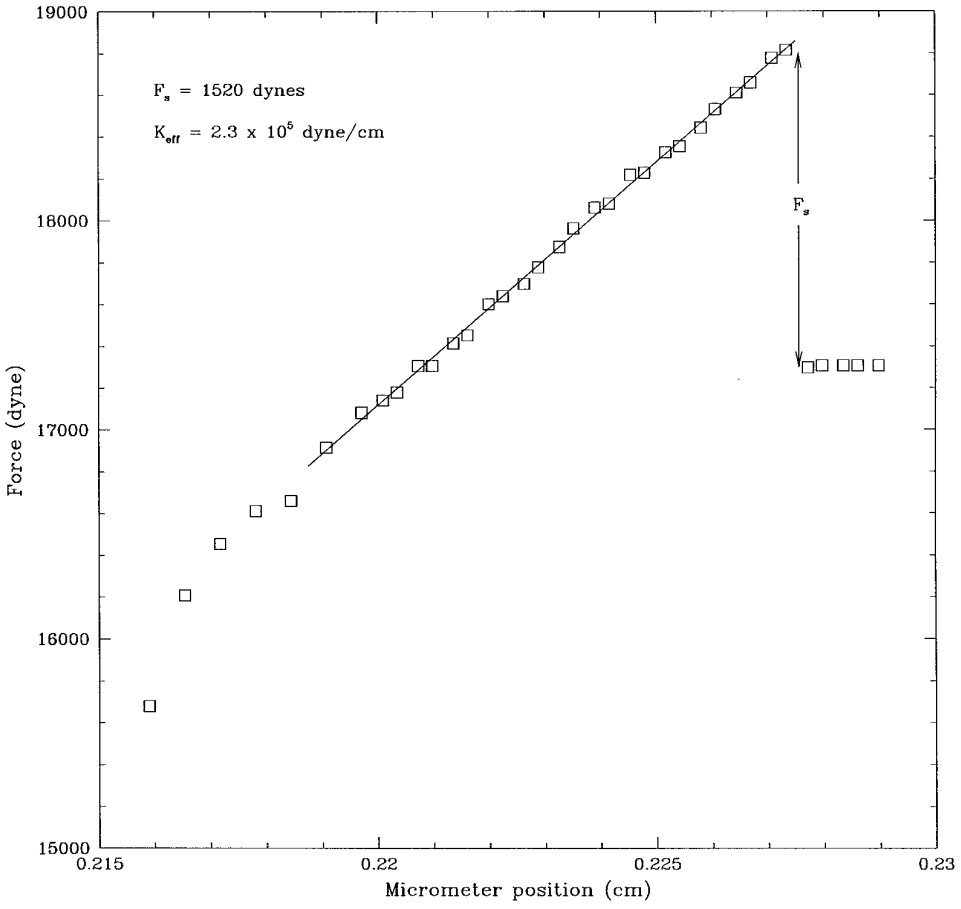

FIG. 4. Force on the load cell as a function of vertical micrometer position for a typical sticking measurement. The frost sticking force, F_s, and the effective spring constant, K_{eff}, determined from the slope of the data via a linear least-squares fit, are indicated.

in Section 2.2. We first present a typical sticking event and explain how the parameters are extracted. In Fig. 4, we plot the force on the load cell as a function of the vertical position as the load cell is raised. We start when the force is close to the weight of the "bob" (we define the bob as the upper plate plus any added weights; for this measurement, the compressive mass was 16 g). There is a change of slope at a force just below the weight of the bob (at higher compression forces, the frost is essentially rigid and does not expand much when the load cell is raised initially). Above this knee in the plot, the frost is acting like a spring, first under compression and then under extension. As the load cell is raised, the force continues to increase until at some point the frost breaks and the measured weight returns to that of the bob alone.

From this data we obtain the sticking force, F_s, as the maximum force minus the bob weight, and the effective spring constant, K_{eff}, from the slope of the curve in Fig. 4. We then calculate the spring constant, K_f, and stretch of the frost, δx_f, from Eqs. (2) and (3).

Errors in K_f and δx_f are small except when the sticking forces are very small. The main errors in K_f and hence in δx_f arise from possible systematic errors in correcting for the spring constant, K_s, of the support string (or wire). This quantity was measured once for each string (or wire) used and then was used for a series of measurements. Variations in K_s from one string/wire to the next were $\lesssim$12%; we estimate that errors in K_f were therefore less than 5%. The errors in F_s are typically 30 dyn and are usually negligible. The scatter in the data for F_s, presented in the following sections, is much larger than the measurement errors, and it is attributed to differences in the frost from one deposition to the next.

3.3. Dependence on Deposition Times and Number of Contacts

We have investigated the sticking behavior as a function of deposition time, keeping other parameters constant, and found that for continuous deposition at a constant flow rate, the maximum measured sticking force for the first

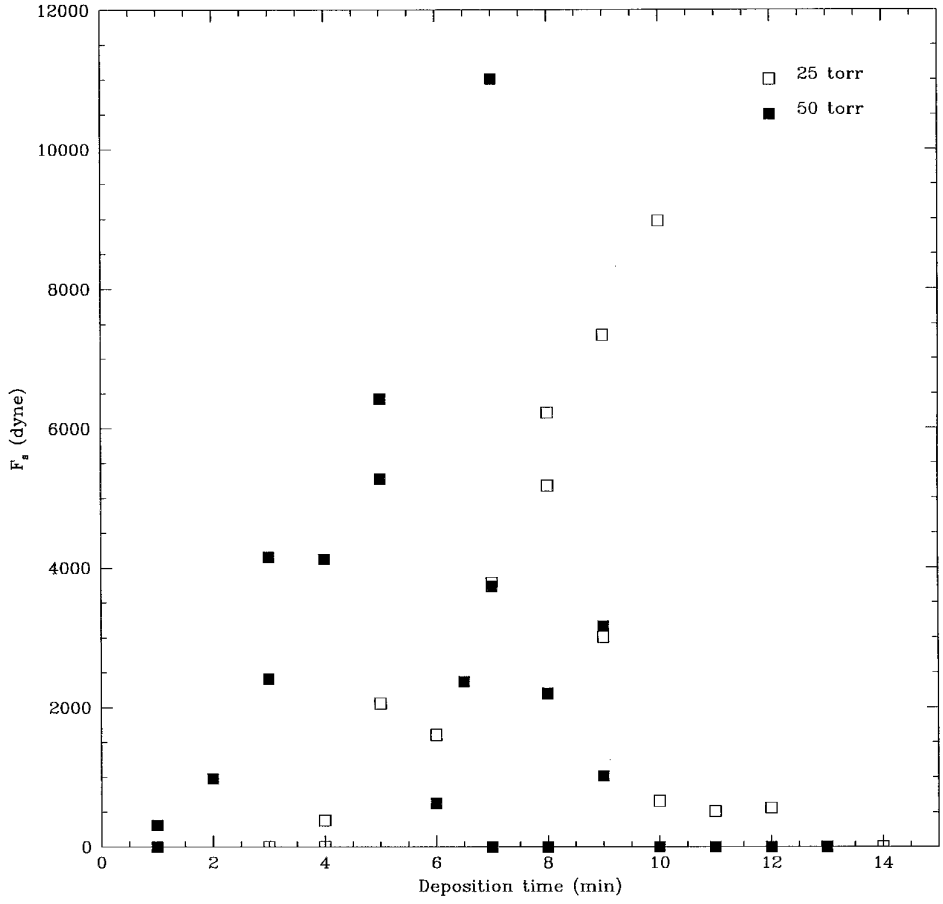

FIG. 5. Frost sticking force F_s as a function of deposition time for two different ambient pressures of nitrogen gas at a flow rate of 22 ml sec^{-1}.

contact increased with the deposition time up to some maximum sticking force. For example, for a flow rate of 22 ml sec^{-1} and a pressure of 50 Torr, the maximum occurs for a 6–7 min deposition as shown in Fig. 5. There is considerable scatter in the data, due in part to variations in the frost layers and in some cases to variations in the adhesion of the frost to the upper and lower plates. For longer deposition times under the same ambient conditions, the observed sticking force drops quickly to near zero values. The same qualitative behavior was observed many times at different temperatures and ambient pressures and for different flow rates. However, the deposition time at which the maximum force occurs depends strongly on the ambient conditions. Qualitatively, when the frost layer becomes too dense (see Section 3.1), the sticking force is greatly reduced.

The sticking force generally decreased with contact number and was usually reduced to zero after 2–6 contacts. However, in a few instances F_s showed an increase on a subsequent contact. Additional deposition of frost, after F_s falls to zero, will again lead to sticking (Fig. 6). In that case, the compressed frost forms the substrate for the second deposition. Therefore, the sticking probability depends on the thickness and density of the porous outer layer rather than on the total frost thickness. This result also suggests that the material in the core of the particle will have little influence on the surface adhesive properties.

3.4. Compressive Force

Sticking measurements were carried out for three compression weights: 1.6, 16 (or 22), and 110 g. These masses correspond to static pressures of approximately 20, 200 (or 275), and 1380 dyn mm^{-2}. In the few cases for which the 110 g weight was used, no sticking was observed, and we conclude that the frost was probably crushed (little dendritic-like structure survived); however, this region in parameter space has not been explored. For the 16 (22) g weight we observed that the maximum sticking force was roughly an order of magnitude larger than for the 1.6 g weight. This supports our earlier proposal (Hatzes *et al.* 1991) that the mechanism for sticking arises from an inter-

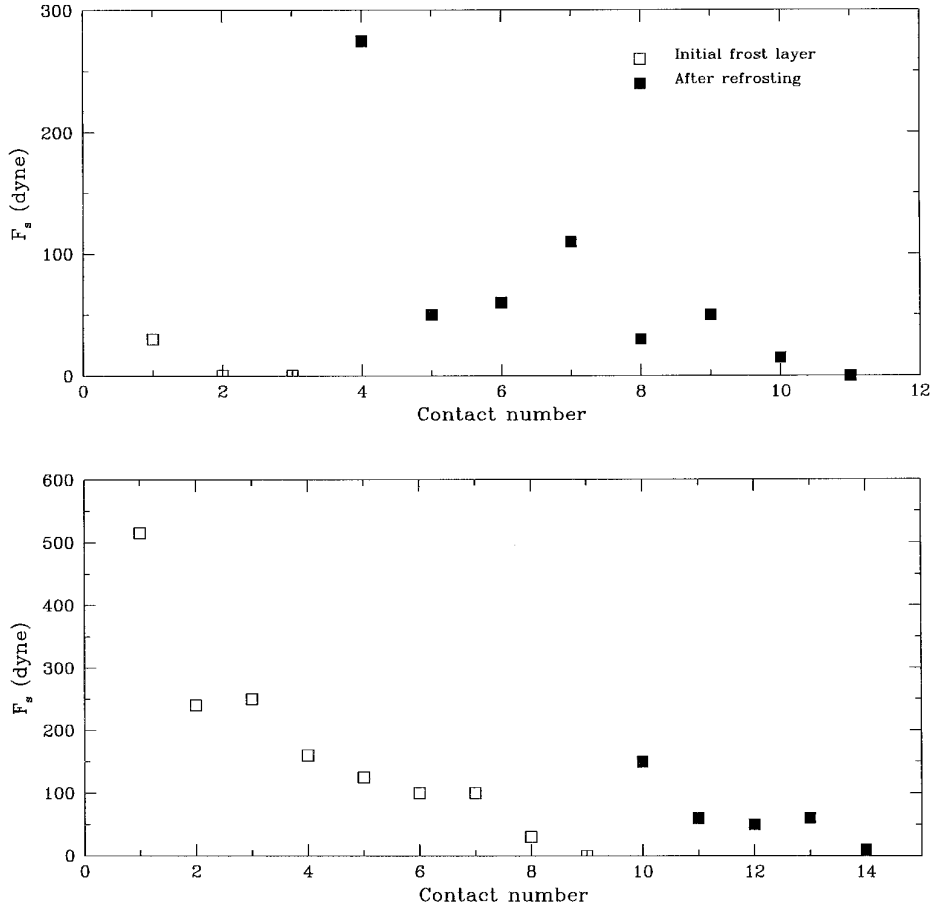

FIG. 6. Frost sticking force F_s versus contact number for two different runs. Open squares represent values of F_s after an initial frosting; solid squares indicate values of F_s from a second frost layer deposited on top of the first. The frosts were prepared at ≈150 K.

penetration of the criss-crossed structure of the two porous frost layers; the interpenetration and hence the resulting sticking force increases with the compression force as long as the frost structure is not significantly damaged.

The compressive force in the solar nebula (i.e., the impulsive force in particle–particle collisions) could be of the same order as the static compressive forces in our experiment. A unit-density sphere of radius 1 cm (m = 4.2 g) impacting a much larger object at a relative velocity v_{rel} = 10 cm sec^{-1} would result in an impulsive force

$$F = \frac{mv_{rel}}{\Delta t} = \frac{(4.2)(10)}{0.6} = 70 \text{ dyn}, \quad (7)$$

where the contact time Δt is estimated from our dynamic experiments with particles with a porous surface frost layer (Bridges *et al.* 1996). If the contact area is ≈1 mm^2, as in our dynamic experiments, then the corresponding pressure is ~70 dyn mm^{-2}, intermediate between the static pressures of the 1.6 and 16 g weights. For surfaces with less frost, Δt can be considerably shorter, and F can be an order of magnitude higher.

3.5. Post-Heating of the Frost Layers

In many experimental runs, the frost was heated by 20–80 K with the two plates in contact (compressed by the 16 g weight) after the first series of contacts at the deposition temperature had reduced the sticking force to zero. The annealing time at the raised temperature was short (typically 15–20 min). In nearly all cases the sticking force was no longer zero if the temperature was raised above 140 K, and in some cases it was higher than the original sticking force for the freshly deposited frost layers. Most of these sticking force measurements were done at the elevated temperature; some were performed at the lower temperature at which the frost was first applied. As an example we present data for frosts deposited near 103 K. Table I shows the sticking force, both for the initial contact and after annealing, for five different 5-min depositions (at 50 Torr with a 22 ml sec^{-1} flow rate). In one case no

TABLE I
The Sticking Force for Five Different Frost Layers

Frost layer	$F_{s,initial}$ (dyn) ($T \approx 103$ K)	$F_{s,annealed}$ (dyn) ($T \approx 140$–180 K)
1	4125	6899
2	0	4361
3	6928	2283
4	1960	0
5	2038	1607

Note. $F_{s,initial}$ is the sticking force on the first contact of the deposited frost. After multiple contacts, the surfaces no longer stick together. $F_{s,annealed}$ is the value after annealing the frost while the two (nonsticking) surfaces were in contact (see text).

sticking was observed for the initial deposition, but sticking was observed after heating to 158 K. Conversely, one case for which sticking was observed for the initial deposition showed no sticking upon heating. In general, annealing the frost to temperatures in the range 140–180 K restored the sticking force to values comparable to those obtained for fresh depositions (but the values appear random), while annealing at lower temperatures (below 130 K) did not produce sticking. This suggests that contact sticking (assumed to be the result of an interpenetration of the two frost layers) and thermally generated sticking (produced by raising the temperature) are comparable in producing adhesion between the surfaces.

Consequently, we attempted to maximize the total observed sticking force by using both mechanisms. We deposited the frost at a temperature near 100 K and then annealed the frost layers while the surfaces were held in contact by the 16 g weight (i.e., no sticking measurement was made for the as-deposited frost). This indeed did lead to larger sticking forces in some cases and produced the largest sticking force we have measured for water frost in this apparatus: 19.4 kdyn.

On the short time scales of our experiment, the sticking forces we measure are elastic. The initial low-temperature adhesion time scales are short, and even during the thermal annealing process there is not sufficient time for diffusion of molecules throughout the frost layer. The increase in sticking force that we observe is likely due to a phase change or to local diffusion just at the interface between the two layers. We observe similar elastic properties in the frost layer both before and after thermal annealing. Viscous effects therefore do not make an important contribution to our measurements.

3.6. Dependence on Ambient Pressure

In the first experiment using a fast flow rate (22 ml sec^{-1}), the 16 g weight, and a relatively high temperature (163 K), we measured the sticking force as a function of deposition time at pressures of 25 and 50 Torr (see Fig. 5). The sticking force is very low for short depositions but then rises (almost linearly with time if one uses the maximum sticking force at each deposition time) to some peak value at a well-defined time. The data are clearly shifted and the position of the maximum occurs at a shorter deposition time (by a factor of roughly 30%) for the higher pressure case. This suggests that the frost is approximately 30% thicker for the 50 Torr deposition for the same deposition time. A general feature of increasing the ambient pressure is to produce a thicker frost layer near the nozzles.

For the slow flow rate (2.4 ml sec^{-1}) and a fixed deposition time of 60 min, we measured the sticking force for ambient pressures between 50 and 400 Torr, again using the 16 g compression weight. In each case we measured the sticking force for the deposited frost at 104 K and then again after annealing at 140 K as outlined in Section 3.5. The results are presented in Fig. 7. For clarity, the data points at 140 K have been shifted to the right (i.e., to higher pressures) by 10 Torr. These results are generally in accord with the faster flow rates reported above. If the peak position moves to a lower deposition time as the pressure is increased, we would observe very little sticking for the higher pressures and would expect a peak at some particular pressure; in this case it occurs for 100 Torr. We expected somewhat more sticking at 50 Torr for the as-deposited frost, but the variation is within the fluctuations we have observed. For the annealed frost we see the same pattern, although there is more sticking at 400 Torr.

3.7. Elastic Properties of the Frost Layers and Impact Strength

The spring constant, K_f, and the total stretch of the frost at the breaking point, δx_f, were determined for a large number (hundreds) of contacts using the method outlined in Section 3.2. The data show that for a wide range of sticking contacts, the spring constant K_f clusters between 10^5 and 10^6 dyn cm^{-1}, irrespective of the frost deposition temperature, the number of contacts, the ambient pressure, or the value of δx_f; in other words, there is little correlation between K_f and δx_f. However, using the largest sticking forces for a set of conditions (i.e., using the values that would form an envelope for the data in Fig. 5), there is a negative correlation. This is likely the result of selecting points with large values of F_s; since $F_s = K_f\, \delta x_f$, F_s can be made large by increasing either K_f or δx_f. (For the largest observed sticking force of 19.4 kdyn, K_f is about average ($\sim 4 \times 10^5$ dyn cm^{-1}), but δx_f is unusually large.)

The stretch of the frost extends over a larger range ($\sim 3 \times 10^{-4}$ to 3×10^{-2} cm) due in part to a general decrease in δx_f with successive contacts. This is seen clearly in Fig. 8, where we plot K_f and δx_f for multiple contacts

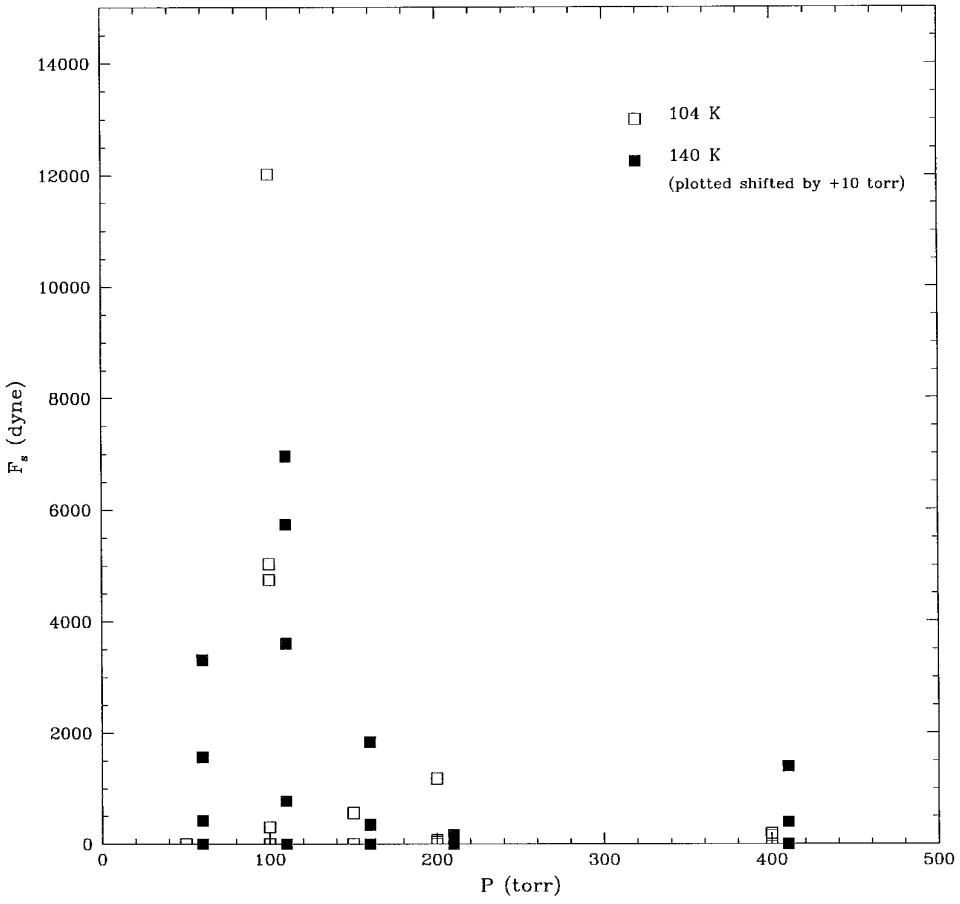

FIG. 7. Frost sticking force F_s as a function of ambient pressure P for annealed frost at 140 K versus that for freshly deposited frost at 104 K.

in six cases for which more than two successive contacts exhibited sticking. The small change (in most cases) in K_f with each successive contact suggests that K_f is a property of that particular frost. The smaller values of δx_f (and correspondingly smaller values of F_s) for multiple contacts indicate a weaker surface adhesion which we attribute to damage to the protrusions at the surface.

To put these results in a larger context, compare the values of K_f in Fig. 8 with an effective spring constant K_{ice} for solid water ice, derived from Young's modulus Y_{ice} for water ice. In general, a tensile stress σ applied to a body produces a longitudinal strain ε proportional to σ (for small stresses) (Hobbs 1974):

$$\sigma = Y\varepsilon. \tag{8}$$

The stress σ is equal to the applied force F per unit area normal to the direction of the force, and the strain ε is the ratio of the stretch δx to the original length x of the body in the direction of F. Therefore, the applied force F can be written

$$F = \left(\frac{YA}{x}\right)\delta x \equiv K_{ice}\,\delta x, \tag{9}$$

where A is the area over which the force is applied. For our frost layers, the thickness of the frost $x \sim 500$ μm (the frost thickness is poorly known; see Section 3.1) and $A \approx 0.78$ cm^2 (Section 2.1). Young's modulus for pure water ice is $Y_{ice} \approx 10^{11}$ dyn cm^{-2} at low temperatures (Hobbs 1974). Therefore, if the frost bond were solid water ice, K_{ice} would be 1.6×10^{12} dyn cm^{-1}. The observed frost bond, with $K_f \sim 5 \times 10^6$ dyn cm^{-1} (Fig. 8), is significantly weaker than solid ice. An estimate of the effective Young's modulus for the frost, Y_{frost}, can be calculated from the equation

$$Y_{frost} = \frac{F}{A}\frac{x}{\delta x}. \tag{10}$$

Using the values $F \sim 5 \times 10^3$ dyn (Figs. 5 and 7), $A \approx 0.78$ cm^2, $x \sim 500$ μm, and $\delta x \sim 30$ μm (Fig. 8), the value

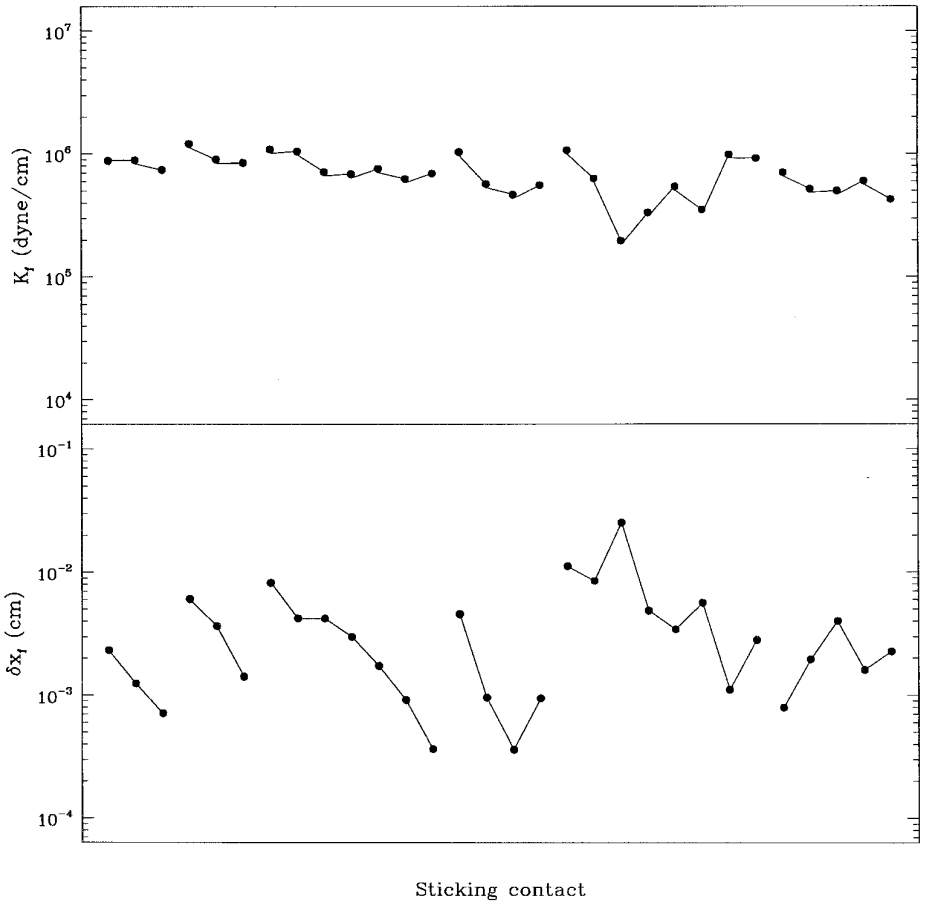

FIG. 8. Frost spring constant K_f and frost stretch δx_f as a function of contact number for six different frost layers. Each connected group of dots corresponds to a single frost layer. For a given group, the first dot represents the initial sticking contact; subsequent dots represent succeeding sticking contacts. After the last sticking contact plotted for a given frost layer, subsequent contacts did not result in sticking. Note that K_f is approximately constant, but that δx_f usually decreases with subsequent contacts.

of $Y_{\text{frost}} \sim 10^5$ dyn cm^{-2}, many orders of magnitude less than Y_{ice}.

A simplistic view of this very small elastic modulus is that the frost is composed of many whiskers, and the cross-sectional area of these whiskers is a small fraction of the plate area. There are two problems with this model. First, the fractional area is extremely small, which means that the whiskers would have to be thin, with diameters much less than 10 μm. (Note that one whisker of ice, of length 500 μm and diameter 20 μm, would have an effective spring constant $\sim 6 \times 10^6$ dyn cm^{-1}, comparable to our measured values.) Second, the total strain is enormous, often >10%. Ice is brittle and will break at much smaller strains.

A more likely scenario is that there are cross-linkages between the whiskers in the frost. In this case, the spring constant is a combination of the bending of the whiskers (as if they were small beams; J. Langer, private communication) and/or the rotations of the points of contact. If we consider the whisker mentioned above as a beam fixed at one end and deflected sideways at the other by δx, then the force is

$$F = \frac{3\pi}{4} \frac{r^4}{x^3} Y \delta x, \tag{11}$$

where r is the whisker radius (10 μm), and x is the length (500 μm). The effective spring constant in this case is

$$K_{\text{eff}} = \frac{3\pi}{4} \frac{r^4}{x^3} Y, \tag{12}$$

and for this ice whisker, $K_{\text{eff}} \approx 2 \times 10^3$ dyn cm^{-1}. Thus, a thousand cross-linkages of this size between protrusions of the two frost surfaces would yield the observed magnitude of spring constant. It is likely that the ends of the

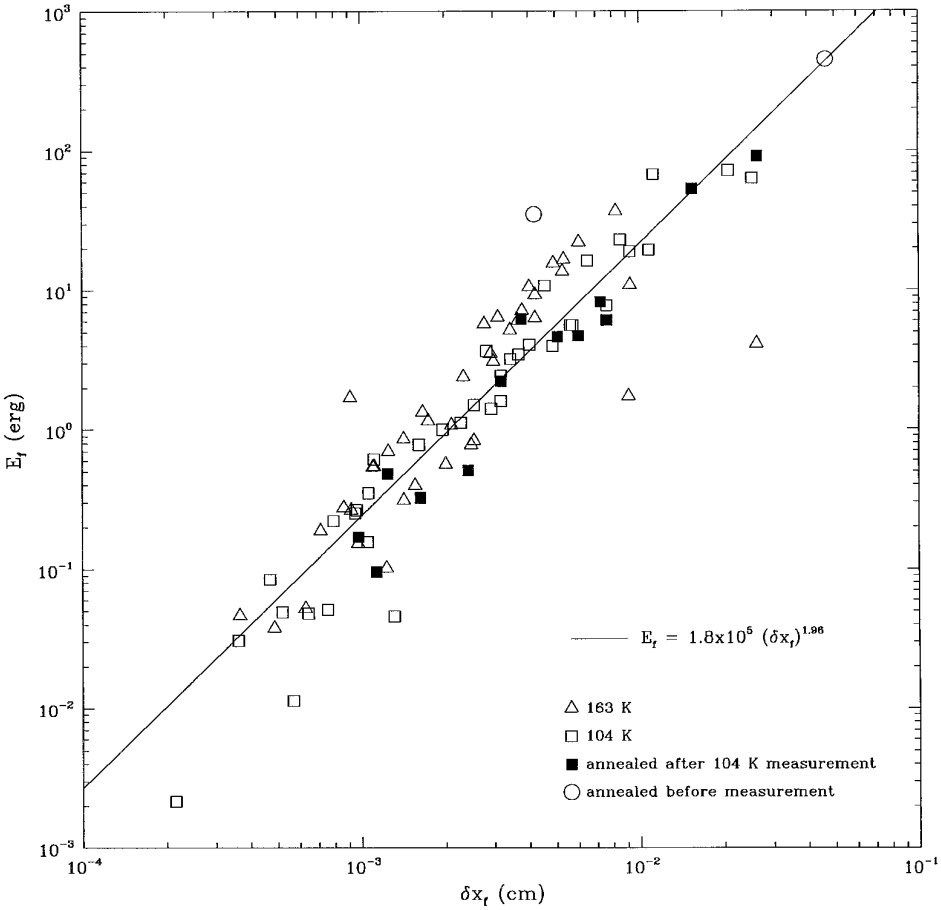

FIG. 9. Stored energy E_f in various frost layers versus frost stretch δx_f. The solid line is a least-squares fit to the data: $E_f = (1.80 \pm 0.93) \times 10^5 (\delta x_f)^{1.96 \pm 0.09}$. The data have a slope of 2, within the errors, in this log-log plot, indicating that the frost spring constant K_f is not strongly dependent on δx_f. The four symbols refer to four different types of frost (see text).

whiskers are not always rigidly attached; this would lower the effective spring constant per whisker. To consider more detailed models, we need to know the size of the whiskers present in the frost.

A more important property of the frost surface, in terms of comparisons with models of protoplanetary formation, is the energy stored in the frost layer, given by

$$E_f = \frac{1}{2} F_s \delta x_f = \frac{1}{2} K_f \delta x_f^2. \quad (13)$$

We plot E_f as a function of δx_f in Fig. 9 for two extensive data sets deposited at 163 K (triangles) and 104 K (squares). The open squares represent data for freshly deposited frost, while the solid squares show the results for frost annealed after the first few contacts, as described in Section 3.5. In addition, we include two points (circles) for which the sticking force was maximized by annealing the frosts while in contact (before any sticking measurement was made), as outlined in Section 3.5. The stored energy shows a strong $(\delta x_f)^2$ dependence, again indicating a nearly constant K_f. Thus for the frosts considered here, the most critical parameter in terms of generating both a large sticking force and a large stored energy is δx_f. To go well above the values of E_f reported here will require higher values of K_f, since the highest values of δx_f are already quite large.

In theoretical models of the development of the Solar System, an important parameter is the impact strength, defined as the energy per unit volume needed to fragment an aggregate (Weidenschilling 1984). In our experiments, most of the (relatively fragile) frosts that exhibited significant sticking have a thickness in the range 300–600 μm. Using 500 μm as a rough average thickness and a contact area of roughly 1 cm^2, the maximum impact strength would be of order 10^4 erg cm^{-3}.

Observations of comets which have fragmented suggest that internal tensile strengths of comets may be very small. Sekanina and Yeomans (1985) conclude that Comet

Brooks 2 had a maximum tensile strength of $\sim 10^3$ dyn cm^{-2}. Comet Shoemaker–Levy 9 may have been even more weakly bound, with a tensile strength of $\sim 10^2$ dyn cm^{-2} or less (Asphaug and Benz 1996, Sekanina 1993). These tensile strengths imply sticking forces much lower than typically observed in our experiment (see Figs. 5 and 7). However, if comets are aggregates of smaller objects, the contact areas between particles would be at least an order of magnitude smaller than the cross-sectional area of an individual particle. Then, using our results, the expected tensile strength for an aggregate held together via frost adhesion at the contact points would range from 50 to 2500 dyn cm^{-2}. These weak tensile strengths cover the range of estimated strengths for both comets; thus one possible model for comets is a collection of smaller particles held together at the contact points via the sticking forces of frost. Alternatively, if the density were more uniform, tidal heating may have played a role in weakening the comets significantly before breakup by causing the release of large amounts of volatiles from their interiors (Ruzmaikina 1996).

3.8. Comparison with Dynamic Experiments

The results from these static sticking experiments compare well with those from our dynamic experiments (Hatzes *et al.* 1991; Bridges *et al.* 1996), in which two frost-coated water ice surfaces collide at relative velocities between 0.01 and 2.0 cm sec^{-1}. The contact area in the dynamic experiments is not as well-defined as in the new experiments, because one contact surface is spherical. The area therefore depends on the frost thickness and the amount of compression. This area is nominally 1 mm^2 but could be as large as 4.5 mm^2 in some cases. In addition, the frost is not compressed uniformly. The spring constant K_f ranges from 10^4 to 10^5 dyn cm^{-1} in the dynamic case. These values are at least an order of magnitude less than the typical K_f in Fig. 8, as expected, since the area over which sticking occurs is $\approx$17–78 times larger in the static case.

The sticking force per unit area for water frost for the static and dynamic cases is also comparable. Most of the dynamic sticking forces F_s for water frost range from several tens to 1000 dyn over an area of a few mm^2, with a maximum F_s of 1500 dyn (Bridges *et al.* 1996). The majority of the static sticking forces F_s have a value of a few thousand dyne over a 0.78 cm^2 area, with a maximum of 19.4 kdyn ($\approx$250 dyn mm^{-2}).

The correspondence between the results of the two experiments is striking, given the fact that they were obtained with two very different apparatuses. In the static experiment, the frost is deposited onto flat substrates composed of metal; in the dynamic experiment, the upper substrate is a water ice surface with radius of curvature 2.5 cm, while the lower substrate is a flat ice surface. The fact that the sticking forces and spring constants (per unit area) are comparable suggests that we are in fact measuring actual properties of water frost, independent of the apparatus used to obtain those parameters.

4. APPLICATION TO PLANETARY PHYSICS

We have shown that contact sticking between frost-coated surfaces occurs for water frosts prepared under a variety of conditions. The main requirements are: (1) that the water frosts have a porous morphology, as in all cases for which a dense, smooth layer was deposited, no contact sticking occurred, and (2) that the temperature is well above 80 K, as frosts deposited at temperatures in the 70–80 K range were extremely powdery and did not even stick to the substrate. The sticking force increases with the compression of the two layers, but for large compressive forces, no sticking occurs. These results support a simple ''Velcro'' model we proposed earlier in which contact sticking arises from an interpenetration of protrusions in the two frost layers (Hatzes *et al.* 1991). Repeated contacts generally damaged the surface layer, but a fresh deposition of order 300 μm thick can restore the surface adhesive properties.

Once frost surfaces are in contact, the magnitude of the sticking force can be greatly increased by short anneals at temperatures in the range 140–180 K. This is true even for surfaces which no longer exhibit sticking after several contacts. Since the increase in temperature is small and the length of the anneal is short, we suggest that a partial transition of amorphous frost to crystalline frost is responsible for this effect.

At temperatures of order 100 K, amorphous frost can form; however, for the relatively fast depositions used in most of these studies, we expect a mixture of crystalline and amorphous frost. The heat of sublimation is given off in the condensation from the vapor phase, and the surface of the frost may be somewhat warmer than the ambient temperature. Amorphous frost, prepared at low temperatures, can change to a crystalline phase when the temperature is raised above $\sim$140 K, but the transition is often not complete, and mixtures of amorphous and crystalline frost have been reported at much higher temperatures (Jenniskens and Blake 1994). A phase transition of this kind involves some displacement of the water molecules and the formation of crystalline bonds, in some cases between sections of the two surfaces that are in physical contact. Thus this sticking mechanism is quite different from the interpenetration model (the ''Velcro'' model) discussed earlier.

In terms of both Saturn's rings and the early stages of development of the solar nebula, water frost can produce sticking in low speed collisions ($v \lesssim 0.5$ cm sec^{-1}; Bridges

et al. 1996) and can hold aggregates together in somewhat higher speed collisions (5–10 cm sec^{-1}). Aggregation via contact sticking of water frost therefore requires nearly laminar and co-linear particle flows for some periods during the aggregate development. If such sticking forces are sufficient to form small aggregates of centimeter-sized particles, and the aggregates persist for some time, then stronger adhesion may develop from inter-surface diffusion and from possible phase changes within the frost, particularly if the aggregates pass through regions of higher temperatures.

We have shown that a temperature rise of only 40–50 K for less than 30 min can generate adhesive forces greater than 10 kdyn cm^{-2} and impact strengths in the range 10^3–10^4 erg cm^{-3}. Longer anneals and repeated thermal cycling should (under some conditions) increase the impact strength further (this will depend on a number of variables, including the amount of amorphous frost present, the area of contact between surfaces at the molecular level, the temperature changes, and the time over which local laminar flow is maintained). We hypothesize that in the solar nebula, collisions between frosty particles (which occur on short time scales) result in an elastic frost bond, which can then undergo thermal annealing as the aggregate moves throughout varying temperature regimes on longer time scales. During such a long annealing process, viscous effects would come into play.

According to recent calculations of particle coagulation in a turbulent solar nebula, aggregate impact strengths need to be at least $\sim 10^5$ erg cm^{-3} (Weidenschilling and Cuzzi 1993). Maximum impact strengths derived from our results are an order of magnitude less than this but could suffice to hold aggregates together if the particles are co-moving and thus have small relative velocities. If the strength of the frost adhesion can increase substantially while the aggregates remain together, as described above, then it is very plausible that in some regions of the solar nebula, water frost as well as other forms of frost might have provided the necessary ''glue'' required for the formation of long-lived centimeter-to-meter size aggregates.

ACKNOWLEDGMENTS

This work was supported in part by NASA Grant NAGW 590 and CalSpace Grant 15500, as well as a Faculty Research Committee grant.

REFERENCES

Anders, E., and N. Grevesse 1989. Abundances of the elements: Meteoritic and solar. *Geochim. Cosmochim. Acta* **53,** 197–214.

Asphaug, E., and W. Benz 1996. Size, density, and structure of Comet Shoemaker–Levy 9 inferred from the physics of tidal breakup. *Icarus* **121,** 225–248.

Bar-Nun, A., I. Kleinfeld, and E. Kochavi 1988. Trapping of gas mixtures by amorphous water ice. *Phys. Rev. B* **38,** 7749–7754.

Beckwith, S. V. W., and A. I. Sargent 1993. The occurrence and properties of disks around young stars. In *Protostars and Planets III* (E. H. Levy and J. I. Lunine, Eds.), pp. 521–541. Univ. of Arizona Press, Tucson.

Blum, J., and M. Münch 1993. Experimental investigations on aggregate-aggregate collisions in the early solar nebula. *Icarus* **106,** 151–167.

Bridges, F. G., K. D. Supulver, D. N. C. Lin, R. Knight, and M. Zafra 1996. Energy loss and sticking mechanisms in particle aggregation in planetesimal formation. *Icarus* **123,** 422–435.

Butler, R. P., and G. W. Marcy 1996. A planet orbiting 47 Ursae Majoris. *Astrophys. J.* **464,** L153–156.

Cameron, A. G. W. 1978. The primitive solar accretion disk and the formation of the planets. In *The Origin of the Solar System* (S. F. Dermott, Ed.), pp. 49–75. Wiley, New York.

Cameron, A. G. W. 1995. The first ten million years in the solar nebula. *Meteoritics* **30,** 133–161.

Chokshi, A., A. G. G. M. Tielens, and D. Hollenbach 1993. Dust coagulation. *Astrophys. J.* **407,** 806–819.

Encrenaz, T., J.-P. Bibring, and M. Blanc 1987. *The Solar System*. Springer-Verlag, New York.

Hartmann, W. K. 1978. Planet formation: Mechanism of early growth. *Icarus* **33,** 50–61.

Hatzes, A. P., F. Bridges, D. N. C. Lin, and S. Sachtjen 1991. Coagulation of particles in Saturn's rings: Measurements of the cohesive force of water frost. *Icarus* **89,** 113–121.

Haynes, D. R., N. J. Tro, and S. M. George 1992. Condensation and evaporation of H_2O on ice surfaces. *J. Phys. Chem.* **96,** 8502–8509.

Hobbs, P. V. 1974. *Ice Physics*. Clarendon Press, Oxford.

Jenniskens, P., and D. F. Blake 1994. Structural transitions in amorphous water ice and astrophysical implications. *Science* **265,** 753–756.

Kerridge, J. F., and J. F. Vedder 1972. Accretionary processes in the early Solar System: An experimental approach. *Science* **177,** 161.

Lock, G. S. H. 1990. *The Growth and Decay of Ice*, pp. 176–177. Cambridge Univ. Press, New York.

Lunine, J. I., and D. J. Stevenson 1985. Thermodynamics of clathrate hydrate at low and high pressures with application to the outer Solar System. *Astrophys. J. Suppl. Ser.* **58,** 493–531.

Lunine, J. I., and W. C. Tittemore 1993. Origins of outer-planet satellites. In *Protostars and Planets III* (E. H. Levy and J. I. Lunine, Eds.), pp. 1149–1176. Univ. of Arizona Press, Tucson.

Marcy, G. W., and R. P. Butler 1996. A planetary companion to 70 Virginis. *Astrophys. J.* **464,** L147–151.

Mayor, M., and D. Queloz 1995. A Jupiter-mass companion to a solar-type star. *Nature* **378,** 355–359.

Miller, S. L. 1961. The occurrence of gas hydrates in the Solar System. *Proc. N. A. S.* **47,** 1798–1808.

Mumma, M. J., P. R. Weissman, and S. A. Stern 1993. Comets and the origin of the Solar System: Reading the Rosetta stone. In *Protostars and Planets III* (E. H. Levy and J. I. Lunine, Eds.), pp. 1177–1252. Univ. of Arizona Press, Tucson.

Palme, H., and B. Fegley, Jr. 1990. High-temperature condensation of iron-rich olivine in the solar nebula. *Earth Planet. Sci. Lett.* **101,** 180–195.

Prinn, R. G., and B. Fegley, Jr. 1989. Solar nebula chemistry: Origin of planetary, satellite, and cometary volatiles. In *Origin and Evolution of Planetary and Satellite Atmospheres* (S. K. Atreya, J. B. Pollack, and M. S. Matthews, Eds.), pp. 78–136. Univ. of Arizona Press, Tucson.

Ruzmaikina, T. 1996. Disruption of SL9 by volatiles released due to tidal heating. *Icarus*, submitted for publication.

Safronov, V. S., 1969. *Evolution of the Protoplanetary Cloud and Forma-*

tion of the Earth and the Planets. Nauka Press, Moscow. [translated for NASA and NSF by Israel Program for Scientific Translation, 1972, NASA TT F-667]

Sekanina, Z. 1993. Disintegration phenomena expected during collision of Comet Shoemaker–Levy 9 with Jupiter. *Science* **262,** 382–387.

Sekanina, Z., and D. K. Yeomans 1985. Orbital motion, nucleus precession, and splitting of Periodic Comet Brooks 2. *Astron. J.* **90,** 2335–2352.

Supulver, K. D. 1997. *Planetesimal Formation in the Outer Solar Nebula*. Ph.D. dissertation, Univ. of California, Santa Cruz.

Weidenschilling, S. J. 1980. Dust to planetesimals: Settling and coagulation in the solar nebula. *Icarus* **44,** 172–189.

Weidenschilling, S. J. 1984. Evolution of grains in a turbulent solar nebula. *Icarus* **60,** 553–567.

Weidenschilling, S. J. 1987. Accumulation of solid bodies in the solar nebula. *Gerlands Beitrage Zur Geophys.* **96,** 21–33.

Weidenschilling, S. J., and J. N. Cuzzi 1993. Formation of planetesimals in the solar nebula. In *Protostars and Planets III* (E. H. Levy and J. I. Lunine, Eds.), pp. 1031–1060. Univ. of Arizona Press, Tucson.